
Bridging Expressivity and Scalability with Adaptive Unitary SSMs

Arjun Karuvally

Salk Institute for Biological Studies
akaruvally@salk.edu

Franz Nowak

ETH Zürich
franz.nowak@inf.ethz.ch

T. Anderson Keller

The Kempner Institute for the Study of Natural
and Artificial Intelligence at Harvard University
t.anderson.keller@gmail.com

Carmen Amo Alonso

Computer Science Department
Stanford University
camoalon@stanford.edu

Terrence J. Sejnowski

Salk Institute for Biological Studies
terry@salk.edu

Hava T. Siegelmann

University of Massachusetts Amherst
hava@umass.edu

Abstract

Recent work has revealed that state space models (SSMs), while efficient for long-sequence processing, are fundamentally limited in their ability to represent formal languages—particularly due to time-invariant and real-valued recurrence structures. In this work, we draw inspiration from adaptive and structured dynamics observed in biological neural systems and introduce the Adaptive Unitary State Space Model (AUSSM): a novel class of SSMs that leverages skew-symmetric, input-dependent recurrence to achieve unitary evolution and high expressive power. Using algebraic automata theory, we prove that AUSSM can perform modulo counting and simulate solvable group automata at finite precision, enabling SSMs to model a broad class of regular languages out of reach for other SSM architectures. To overcome the practical inefficiencies of adaptive recurrence, we develop a separable convolution formulation and a CUDA implementation that enables scalable parallel training. Empirically, we show that AUSSM and its hybrid variant—interleaved with Mamba—outperform prior SSMs on formal algorithmic tasks such as parity and modular arithmetic, and achieve competent performance on real-world long time-series classification benchmarks. Our results demonstrate that adaptive unitary recurrence provides a powerful and efficient inductive bias for both symbolic and continuous sequence modeling.

1 Introduction

Modeling long-range dependencies efficiently and expressively remains a central challenge in sequence modeling. While Transformer architectures have achieved state-of-the-art results across domains such as language modeling [1, 2, 3], forecasting [4, 5], and protein design [6], their quadratic complexity with respect to sequence length limits scalability [7]. In response, recent work has explored *state space models* [8, 9] (SSMs) as a scalable alternative, using linear-time convolutions and structured recurrence to enable efficient processing of long sequences [9, 10]. Despite the computational advantages SSMs offer, they are fundamentally limited in their ability to express general linear time-varying systems and formal languages efficiently. Even basic regular languages that require counting, such as parity or balanced parentheses [11] are impossible for practically used

Preprint. Under review.

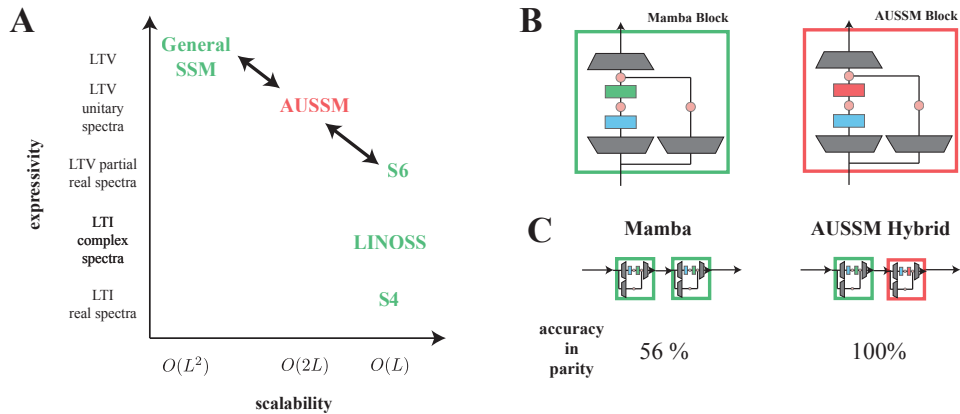


Figure 1: **AUSSM uses adaptive linear time varying (LTV) recurrence with unitary spectrum balancing scalability and expressivity.** **A.** Existing practical SSMs use $O(\log L)$ time complexity algorithms for computing the output in parallel. These algorithms require additional memory that determines their scalability, resulting in a tradeoff with expressivity. General SSMs with dense LTV (fully adaptive) recurrences and non-diagonalizable matrices are the most expressive but lack scalable computational algorithms and suffer from gradient issues. AUSSM balances the expressivity-scalability tradeoff using a fully adaptive diagonal unitary recurrence. The result is a $O(2L)$ (we keep the constant factor in the asymptote to explicitly show that the algorithm requires higher memory) complexity SSM without gradient issues and higher expressivity than practical SSMs. **B.** The AUSSM block uses the same block structure as Mamba [10], where the S6 SSM in Mamba is replaced with AUSSM. **C.** AUSSM blocks can be used as drop-in replacements for existing SSM backbones to provide higher expressivity, as depicted by the performance improvement in the parity task.

SSM architectures like Mamba that has positive real eigenvalue spectra. Frontier SSMs are either Linear Time Invariant (LTI), or partially Linear Time Varying (LTV), resulting in weaker expressivity compared to more general LTV systems that are capable of approximating any non-linear dynamical systems [12]. Two properties thus emerge as necessary for increasing the expressivity of SSMs: a general eigenvalue spectrum and adaptive recurrence. However, incorporating both these properties naively in SSMs introduces gradient instability through the exploding/vanishing gradient problem [13], and leads to quadratic computational complexity, severely limiting scalability.

In this work, we propose the *Adaptive Unitary State Space Model* (AUSSM) as a principled middle ground between scalability and expressivity. AUSSM is a **fully adaptive state space model** with linear time-varying recurrence and a unitary eigenvalue spectrum, combining the theoretical benefits of time-varying recurrence with the practical advantages of structured, conserved dynamics. We formally prove that AUSSM can perform modulo counting with constant-width hidden states, and that combining AUSSM with existing non-adaptive models like Mamba yields *maximal expressivity within the class of diagonal SSMs*. To make this architecture scalable, we introduce a novel *separable kernel formulation for adaptive SSMs* that exposes efficient computational algorithms which reduce the quadratic cost of adaptive recurrence to linear time and space. Empirically, we validate the theoretical claims through a suite of algorithmic tasks, demonstrating substantial performance gains over Mamba, and showing that AUSSM retains competitive efficiency through an optimized CUDA implementation. Further, we evaluate the long-range modeling capabilities by testing on a suite of time series benchmarks.

Interestingly, structured unitary and adaptive dynamics are also found as emergent behavior in biological neural systems [14] and even trained non-linear recurrent neural networks [15], where they are believed to support flexible integration of information over space and time [16]. We take the computational role of these structured unitary dynamics as a motivation to derive AUSSM using a skew-symmetric ODE used in identifying purely rotational features from data in neuroscience [17].

AUSSM provides a new architectural foundation that bridges formal expressivity and practical scalability (Figure 1). It expands the space of scalable SSMs by showing that adaptive (and time-varying) recurrences can be made computationally efficient, unlocking new capabilities for symbolic and long-context sequence modeling that is grounded in biological principles and theory.

2 Background and Motivation

State Space Models (SSMs) have emerged as efficient alternatives to Transformers for sequence modeling, particularly in long-context settings. SSMs compress arbitrarily long sequences into a fixed-dimensional hidden state using a recurrent formulation and this can be computed in parallel using an efficient convolution formulation.

The most general SSMs are described by a continuous-time Ordinary Differential Equation (ODE):

$$\frac{dx(t)}{dt} = A_t x(t) + B_t u(t), \quad y(t) = C_t x(t) \quad (1)$$

or its discrete counterpart:

$$x(t) = A'_t x(t-1) + B'_t u(t), \quad y(t) = C'_t x(t) \quad (2)$$

where $x(t) \in \mathbb{R}^n$ is the hidden state, $u(t)$ is the input, and $y(t)$ is the output. The matrices A_t, B_t, C_t define the system dynamics and may vary over time. In the discrete system, these matrices have an equivalent discretized counterpart in A', B', C' , respectively. The discrete recurrence can be reformulated as a parallel convolution:

$$y(t) = \sum_{k \leq t} C'_t (A'_{t-1} \cdots A'_{k+1}) B'_k u(k) \quad (3)$$

This enables efficient parallel processing, but storing a general convolution kernel requires $\mathcal{O}(L^2)$ memory for sequence length L , as each kernel entry must be stored for t and k that index over the sequence length. To avoid this, most practical SSMs assume time-invariant dynamics ($A_k = A, B_k = B, C_k = C$), allowing for a compressed storage of the kernel but significantly restricting expressivity. Recent SSMs like Mamba [10] introduce *mild adaptivity*, where B, C , and step size Δ are adaptive while keeping A fixed or diagonal. However, such models cannot simulate general Linear Time-Varying (LTV) systems or perform counting-based tasks (e.g., parity, modular arithmetic) with constant-width hidden states (see Appendix A). These limitations prevent Mamba from modeling input-sensitive dynamics or general multiscale time-varying behavior. There are other approaches that try to improve the expressivity of SSMs by generalizing real-valued recurrences. Notably, Linear Recurrent Units [18] generalize the real-valued eigenvalue spectra with initialization close to the unit circle on the imaginary plane. This formulation has been shown to be capable of universal approximation when interleaved with non-linear multi-layer perceptrons [19]. However, this approximation relies on perfectly storing the dynamical system history without regard to resource constraints. General LTV systems are much more flexible as they have the capability to gate information based on input, thereby retaining only selected information (compressed information) that is necessary for processing rather than a lossless history. Another notable work is linear Oscillatory State Spaces (linOSS) [20], where simple harmonic ODEs are discretized to derive novel oscillatory SSMs with conservation properties identical to AUSSM. The linOSS models are more expressive than SSMs with purely real eigenvalues, but fall short of an LTV system. AUSSM balances the two - the improved expressivity of diagonal LTV systems and the scalability of separable convolutions.

3 Adaptive Unitary State Space Model (AUSSM)

We tackle the problem of balancing expressivity with scalability in Adaptive State Space Models by introducing two features. Adaptive input-dependent recurrent matrix improving expressivity, and unitary dynamics addressing training scalability. In this section, we derive AUSSM from the skew-symmetric ODE used to identify rotational features in the brain [17], then we prove that the inputs control AUSSM rotational frequencies smoothly, enabling a stable and effective adaptive SSM. Next, we prove that the AUSSM is maximally expressive in the class of regular languages.

To derive the AUSSM model with purely rotational properties, we use the skew-symmetric Ordinary Differential Equation (ODE) used in the rotational Principal Component Analysis (jPCA) procedure - a variant of Principal Component Analysis (PCA) used in neuroscience [17]. jPCA is used to identify rotational features of a dynamical system using observations from it. Since our requirement is to process an input signal $u(t)$ into the hidden state, we use a version of the jPCA ODE with control input given by Equation 1, with the additional constraint that the input matrix A_t is skew-symmetric (with purely imaginary eigenvalues) and B_t and C_t stay constant with time, i.e., $B_t = B$ and $C_t = C$.

We discretize the ODE using the ZOH discretization procedure with a step size $\Delta_t \in \mathbb{R}$ to obtain a discrete dynamical system (See Appendix B for details),

$$\begin{cases} x(t) = \exp(\Delta_t A_t) x(t-1) + \Delta_t B u(t), \\ y(t) = C x(t). \end{cases} \quad (4)$$

Note here that A_t changes with time from adaptivity, and it is a skew-symmetric matrix. We assume that $A_t, \forall t$ belongs to a class of simultaneously diagonalizable matrices. Therefore $\exp(\Delta_t A_t)$ can be diagonalized to obtain $\exp(\Delta_t i\Lambda_j(t))$ where $\Lambda_j(t) \in \mathbb{R}$ and each $i\Lambda_j(t)$ is the j^{th} eigenvalue of the matrix A_t . This implies that the final discrete dynamical system has purely unitary eigenvalues, i.e., eigenvalues exactly on the unit circle. The AUSSM ODE is a marginally stable, time-varying linear system where the input both drives and dynamically reshapes the system. The skew-symmetric nature of A_t guarantees marginal stability by ensuring that all eigenvalues lie on the imaginary axis in continuous time, or on the unit circle after discretization (see Lemma 4 in Appendix C). This structure enables long-term memory retention without gradient explosion or decay (see Lemma 5 in Appendix C)¹.

The adaptivity of A_t is enforced by making A_t be a function of input with $A_t = f(u(t))$ where $f : \mathbb{R} \rightarrow \mathbb{R}^n$ is the function defining how the input influences the recurrent matrix. With adaptivity, the input acts as a control signal, shaping the rotational dynamics based on the instantaneous input, analogous to gain scheduling or bilinear control systems [21, 22]. This design allows the system to dynamically traverse a spectrum of rotational behaviors in the state space, facilitating expressive temporal modeling driven by the input signal.

Theorem 1 (Input-Modulated Rotation Frequencies via Skew-Symmetric Generator). *Let $A : \mathbb{R} \rightarrow \mathbb{R}^{n \times n}$ be a smooth function such that $A(u)$ is skew-symmetric for all $u \in \mathbb{R}$. Then for each $u \in \mathbb{R}$, all eigenvalues of $A(u)$ lie on the imaginary axis, and the eigenvalues of the discrete-time transition matrix $\Phi(u) = \exp(\Delta A(u))$ lie on the complex unit circle. Furthermore, the eigenvalues of $A(u)$ depend continuously on u , and thus the angular frequency of state-space rotation is smoothly and directly modulated by the input. See proof in Appendix C.*

Hence, by designing $A(u)$ appropriately (e.g., via a learnable function $f(u)$), the AUSSM can modulate the rotational speed and mode structure of the hidden state space based on the input signal in a smooth and controlled manner. Further details on how the above SSM is practically implemented are in Section 4, where we diagonalize the above ODE and introduce input adaptivity. The inputs also have a dimension of d , in which case the proposed SSM is applied to each input dimension following the approach used in Mamba.

Formal Expressivity *Given our construction of the AUSSM, how expressive is it for formal languages?* Representing simple formal languages has been found to be a major weakness of SSMs. Recently, a flurry of research has utilised algebraic automata theory, specifically Krohn-Rhodes theory [23], to analyze the types of formal languages expressible by different LLM architectures, notably transformers [24] and SSMs [11, 25]. The Krohn–Rhodes decomposition theorem states that any finite-state machine can be simulated by a cascade of simpler automata drawn from two types: permutation automata, which model reversible group-like behavior, and reset automata, which model state-resetting dynamics (the next state depends only on the input, not on the current state). This result implies that complex regular languages can be recognized by composing SSMs that simulate these simple automata. There is a subset of finite-state automata whose decomposition contains only set-reset automata and *cyclic* permutation automata, which suffices to recognize a large subset of regular languages, the so-called solvable languages.

Most SSMs used in practice have diagonal or diagonalizable transition matrices A that can only have positive eigenvalues. As [11] showed, this means they cannot perform modulo counting, restricting their expressivity to the subset of star-free regular languages. [11] also outlines the necessary conditions for SSMs to overcome this limitation and represent a larger class of regular languages. This requires 1. the ability to implement modulo counters, and 2. the ability to implement Krohn-Rhodes cascade products. Here, we reiterate their relevant results and show that our implementation not only satisfies these conditions but can recognize any solvable regular language, a language class out of reach for most practical SSMs.

¹In practice, there will always be small deviations from the ideal theoretical behavior due to limited precision of modern computers.

Fact 1 ([11], Thm. 2). *Diagonal (or diagonalizable) SSMs with only positive eigenvalues cannot perform modulo counting, which means they can only recognize star-free languages.*

Lemma 1. *For any $k \in \mathbb{Z}^+$, one can construct a single-layer AUSSM that counts modulo k , which means AUSSMs can simulate arbitrary cyclic permutation automata.*

Proof sketch. Assume we want to count the number of 1’s modulo 2 in a length- T input sequence $(u)_{t=1,\dots,T} \in \{0, 1\}^T$. A single-layer AUSSM with $x_0 = 1$, $A(1) = -1$, $A(0) = 1$, and $B(0) = B(1) = 0$ will have a hidden state of $x_t = -1$ for odd counts and $x_t = 1$ for even counts of 1 up to position t . Similarly, to count modulo 4, we can set $A(1)$ to the fourth root of unity, i.e., either i or $-i$, and $A(0) = 1$, $B(0) = B(1) = 0$, as before. This method can be extended to other mod k counters by setting $A(1)$ to the k th root of unity, $\exp(2\pi i/k)$. An AUSSM can take on these parameters as it uses input-dependent A matrices whose eigenvalues lie on the unit circle of the complex plane.² This technique can be extended to perform modulo k addition, which allows the simulation of cyclic permutation automata (see App. D). \square

Lemma 2. *An SSM consisting of interleaved Mamba and AUSSM blocks (hybrid Mamba+AUSSM) can implement cascade products of automata simulated by Mamba SSMs and AUSSMs.*

Proof sketch. [11, Lem. 19] showed that multilayer Mamba SSMs can implement cascade products of Mamba layers simulating set-reset automata, which, by Schützenberger’s theorem [26], means they can recognize any star-free language. This can easily be extended to show that any automaton simulated by Mamba or AUSSM layers can be joined into a cascade product within alternating Mamba and AUSSM blocks. This works because we can always add additional padding layers at any point in the hybrid SSM without changing the behavior of the remainder of the SSM. \square

Corollary 1. *Hybrid Mamba+AUSSM can recognize any solvable language, that is, any regular language whose syntactic monoid does not contain non-solvable subgroups.*

Proof sketch. By Lem. 1, an AUSSM layer can simulate cyclic permutation automata, and [11, Lem. 19] showed that a Mamba layer can simulate set-reset automata. Now, the Krohn-Rhodes theorem states that every finite automaton divides a cascade of alternating aperiodic monoids (set-reset automata) and finite simple groups (permutation automata). A finite group is solvable iff its decomposition series contains only cyclic groups of prime order (cyclic permutation automata with prime-length cycles) [27, Ex. 3.4.8]. By Lem. 2, hybrid Mamba+AUSSM can implement the Krohn-Rhodes cascade product of set-reset automata (Mamba) and cyclic permutation automata (AUSSM). Therefore, it can recognize all solvable languages. (cf. [11, Thm. 21]). \square

Regular languages that require representing more complex non-solvable group transformations, such as the word problem in S_5 or A_5 , lie outside of this set, and according to widely held assumptions about complexity theory, cannot be modeled by diagonal SSMs [28]. This means combining Mamba with AUSSM maximises the representational capacity of diagonal SSMs (short of lifting the diagonal transition restraint, which leads to poor scaling).

4 Separable Convolution Kernels for Scalable Adaptive SSMs

One of the main challenges in designing SSMs, is the computational efficiency of the implementation. Simulating the discrete dynamical system in Equation 4 naively is not computationally efficient as it leads to quadratic memory scaling when it is parallelized using the typical SSM convolution procedure (Appendix E.1). In this section, we introduce a separable kernel formulation that exposes efficient computational implementations for adaptive SSMs. A related approach to ours is the recently proposed semiseparable matrix formulation [29], where a special class of matrices is shown to have efficient computation algorithms. Our formulation works directly in the convolution form of the SSM and instantly exposes the separability and is applicable to a wider class of adaptive SSMs as shown below. We note here that the separable kernel formulation is not specialized for the AUSSM, but

²We assume an idealised setting, disregarding rounding errors from floating point precision, for simplicity. For most sequence lengths seen in practice, rounding errors are indeed negligible (see App. D for details).

applies to a class of SSMs that are simultaneously diagonalizable [30]. We therefore formulate the theory in the general case and provide sufficient conditions to apply the theory in practice.

The general convolution formulation of general SSMs in Equation 3 is typically used to convert a discrete dynamical system form of an SSM to an efficient parallel implementation. This form is abstracted as applying a convolution on the input, following the equation

$$y(t) = \sum_{k \leq t} K(t, k) u(k). \quad (5)$$

The reason for the quadratic memory scaling of the convolution operation can be observed in this abstracted form as storing the $K(t, k)$ convolution kernel requires, in general, $O(L^2)$ memory, where L is the sequence length.

Separable convolution kernels have the additional property that $K(t, k) = f(t)g(k)$ that enables writing the output as

$$y(t) = f(t) \sum_{k \leq t} g(k) u(k). \quad (6)$$

Storing the additional $f(t)$ and $g(k)$ requires only an additional $O(2L)$ memory, compared to $O(L)$ for the non-adaptive case, producing asymptotic memory efficiency matching that of the non-adaptive SSM with only a constant factor scaling. The above convolution formulation can be efficiently computed in $O(\log(L))$ time by using the parallel prefix sum algorithm [31]. It is instructive to apply this formulation to an existing SSM to identify efficient computational structures - we use the partially adaptive Selective State Space Model (S6) used in the popular Mamba model [10].

Separable Convolution Formulation of Mamba Selective SSM (S6): In S6, the matrices C and B vary with input (making the SSM selective to input), in addition to the step size Δ varying with time. This generalization results in the output of the SSM written in the convolution form as:

$$y_{ti} = \sum_{k \leq t} \sum_j C_{tj} \exp((t\Delta_{ti} - k\Delta_{ki})A_j) \Delta_{ki} B_{kj} u_i(k). \quad (7)$$

Here, the input $u \in \mathbb{R}^d$ is a vector and the SSM is applied to each input dimension in parallel. The index i is over the input dimension d , and j indexes the hidden state dimension n . In the general convolution formulation we showed above, the S6 output is formulated as applying the convolution kernel $K(t, k) = C_{tj} \exp((t\Delta_{ti} - k\Delta_{ki})A_j) \Delta_{ki} B_{kj}$ on the inputs over time u_i . Note here that, unlike typical time-invariant SSMs, the S6 convolution kernel is unique to each y as Δ, B, C change with time. Since $K(t, k) = \left(C_{tj} \exp(t\Delta_{ti}A_j) \right) \left(\exp(-k\Delta_{ki}A_j) \Delta_{ki} B_{kj} \right)$, the kernel is separable and we can use the procedure we introduced above to compute the S6 output in a time and memory-efficient manner (see Appendix F.1 for an efficient Pytorch Implementation of the S6).

Separable Convolution Formulation of AUSSM: In the case of S6, the separable formulation was easily revealed directly from the convolution form. In the case of AUSSM, this separability is not possible for the most general case. However, when the set of recurrent matrices A_t is simultaneously diagonalizable, the output of the AUSSM in Equation 4 can be formulated as (See Appendix B for details)

$$y_{ti} = \Re \left[\sum_{k \leq t} \sum_j C_j \exp \left(\mathbf{i} \sum_{l \leq t} \theta_{A_{li}} \right) \frac{\Delta_{ki} B_j}{\exp \left(\mathbf{i} \sum_{l \leq k} \theta_{A_{li}} \right)} u_i(k) \right]. \quad (8)$$

Here, $\theta_{A_{li}} = \sum_r x_{ijr} u_r(k) + x_{ij}^{\text{bias}}$ is the angle argument of the unitary discretized A' matrix in the polar form. Note here that as the AUSSM has complex eigenvalues, the final output is also complex, and we use only the real part of the output with the function $\Re[\cdot]$. With this formulation of the AUSSM recurrence, a memory and time efficient computation of the adaptive SSM is obtained, however, implementing this convolution directly in Pytorch can still result in high memory usage as the constant in the $O(L)$ is bdn where b is the batch size, d is the input dimension and n is the hidden dimension resulting in a large constant factor. We therefore create a CUDA kernel, where this additional complexity is hidden and the hidden state is only partially materialized in the CUDA kernel (Appendix F.2).

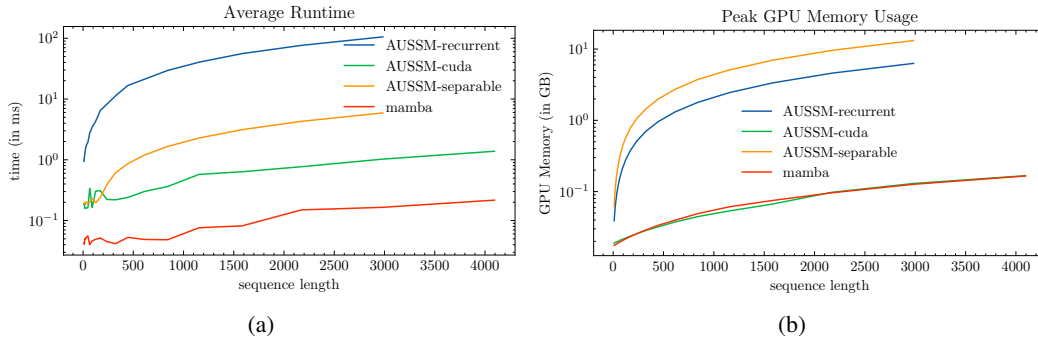


Figure 2: **AUSSM with separable convolution achieves efficient runtime and memory scaling for fully adaptive SSMs.** The runtime and peak memory usage of four implementations are compared: recurrent PyTorch AUSSM, separable PyTorch AUSSM, our optimized CUDA AUSSM kernel, and the Mamba CUDA kernel. (a) The AUSSM CUDA implementation outperforms both PyTorch baselines in speed and memory efficiency, and approaches the memory efficiency of Mamba despite AUSSM’s full adaptive recurrence. Notably, the Pytorch implementation of the separable convolution has better runtime efficiency compared to the recurrent implementation, albeit at a higher memory cost. (b) The AUSSM CUDA kernel has a significantly lower memory footprint, identical to that of the partially adaptive and optimized mamba CUDA kernel.

5 Experiments

We empirically validate the theoretical claims of AUSSM by evaluating both its computational efficiency and expressivity. First, we benchmark runtime and memory usage across four implementations, including our CUDA-optimized AUSSM and Mamba. Second, we assess expressivity on a suite of algorithmic tasks requiring formal language recognition, such as parity and modular arithmetic. Finally, we evaluate real-world applicability on long-sequence classification and regression tasks, demonstrating that the improved expressivity of AUSSM translates to practical performance gains.

5.1 Scalability Evaluation

We benchmark four implementations of AUSSM to assess efficiency: (1) a naive PyTorch recurrent version, (2) a PyTorch version using separable convolutions with a higher constant factor in the linear scaling, (3) our custom CUDA kernel, and (4) the Mamba CUDA kernel as a baseline. Experiments were run on a single NVIDIA 2080 Ti GPU with 11 GB VRAM. As shown in Figure 2, the CUDA-based AUSSM achieves significantly lower memory usage and faster inference compared to the PyTorch variants, approaching the efficiency of Mamba despite full adaptivity. The separable PyTorch implementation improves runtime over the recurrent baseline but incurs higher memory costs. Overall, our separable formulation paired with a low-level CUDA kernel enables AUSSM to scale to long sequences efficiently, validating the theoretical benefits of scalability.

5.1.1 Expressivity Evaluation

To evaluate formal expressivity, we benchmark AUSSM, Mamba, xLSTM [32], and a hybrid AUSSM+Mamba model on a suite of algorithmic tasks drawn from various levels of the Chomsky hierarchy. These include tasks requiring counting (e.g., parity, modular arithmetic), memory manipulation (e.g., repetition), and symbolic reasoning (e.g., equation solving). Models are trained on sequences up to length 40 and tested on lengths up to 256 to assess length generalization performance. We evaluate all the models using scaled validation accuracies to account for the differing number of output classes in the algorithmic tasks.

The results are shown in Table 1. The AUSSM achieves perfect accuracy on tasks that require modulo counting and cycle tracking, validating its theoretical ability to simulate cyclic permutation automata via unitary and adaptive dynamics. In contrast, Mamba fails to generalize on these tasks, consistent with the limitations of partially adaptive and dissipative models. However, AUSSM performs poorly on tasks such as majority or equation solving, where dissipative dynamics may be required for stability and information aggregation. Notably, the AUSSM hybrid model performs significantly better than

Complexity Class	Task	xLSTM	Mamba	AUSSM	AUSSM Hybrid
Context Sensitive	repetition	0.09	0.15 ³	0.1993 ²	0.45¹
	bucket sort	0.7 ³	0.69	0.92¹	0.83 ²
	majority count	0.5¹	0.45 ²	0.096	0.37 ³
	majority	0.64 ²	0.69¹	0.57	0.64 ²
Deterministic Context Free	solve equation	0.24¹	0.05	0.07 ²	0.07 ²
	mod arith	0.15 ²	0.04	0.13 ³	0.23¹
Regular	mod arith wo bra	1.0¹	0.13	0.48 ³	0.53 ²
	cycle nav	0.8	0.86 ²	1.0¹	1.0¹
	parity	1.0¹	0.13 ²	1.0¹	1.0¹

Table 1: **AUSSM and hybrid AUSSM+Mamba models outperform Mamba on tasks requiring counting and structured memory.** We evaluate xLSTM, Mamba, AUSSM, and a hybrid AUSSM+Mamba model on a suite of algorithmic reasoning tasks. The table shows the scaled test accuracies on each task. The tasks are grouped by their position in the Chomsky hierarchy. AUSSM achieves perfect accuracy on tasks like parity and cycle navigation, which require modulo counting, validating its theoretical expressivity. While Mamba performs better on tasks such as majority count, the hybrid model consistently achieves the best or near-best performance across most tasks, demonstrating that combining adaptive unitary dynamics with real-valued recurrence yields a more expressive and general-purpose architecture. The scaled accuracies for xLSTM and Mamba are obtained from [32].

Dataset	Heartbeat	SCP1	SCP2	Ethanol	Motor	Worms	Avg
Seq Length	405	896	1152	1751	3000	17984	
Num Classes	2	2	2	4	2	5	
S5	47.8 ± 3.1	74.2 ± 2.1	10.2 ± 3.3	0.8 ± 3.5	6.0 ± 3.9	79.9 ± 4.1	36.4
S6	53.0 ± 8.3¹	65.6 ± 2.7	-0.2 ± 9.4	1.9 ± 6.4	2.6 ± 4.7	81.3 ± 6.2	34.0
linoss	51.6 ± 3.7	75.6 ± 2.6¹	17.8 ± 8.1¹	6.5 ± 0.6¹	20.0 ± 7.5¹	93.8 ± 4.4¹	44.2¹
Mamba	52.4 ± 3.8	61.4 ± 1.4	-3.6 ± 3.9	3.9 ± 4.5	-4.6 ± 4.5	63.6 ± 15.8	28.8
AUSSM Hybrid	53.0 ± 3.8¹	64.2 ± 4.9	4.2 ± 6.8	4.7 ± 4.1	2.6 ± 5.5	82.6 ± 3.4	35.2

Table 2: **Hybrid AUSSM with Mamba achieves competent performance on long time-series classification benchmarks.** We evaluate the hybrid model on six UEA datasets spanning a wide range of sequence lengths and domains. The table shows the scaled test accuracies for the different models compared to the hybrid AUSSM. The hybrid AUSSM consistently outperforms the base mamba and achieves competent accuracy across datasets. These results demonstrate that the increased expressivity of AUSSM, when combined with Mamba’s stability, translates into strong real-world performance even on long and complex sequence data. Our model is evaluated on a statistically rigorous test with 20 different seeds to obtain a better estimate of test accuracy to reduce the reliance on arbitrary evaluation seeds used in prior works [20].

all existing RNNs, including the xLSTM, suggesting that AUSSMs and Mamba blocks are synergistic and exhibit performance benefits that neither individual model provides. These results empirically support our theoretical claim that hybrid models combining AUSSM and Mamba maximize the expressivity of diagonal SSMs under the Krohn–Rhodes framework.

5.2 Long Time-Series Classification and Regression Benchmark

To evaluate the practical benefits of our architecture, we test the hybrid AUSSM+Mamba model on a suite of UEA long-time-series classification benchmarks [33] and the challenging Weather regression benchmark. We take the AUSSM block as a drop-in replacement for an existing Mamba backbone. Specifically, we randomly selected a fixed number of Mamba blocks in a deep Mamba SSM model and replaced them with the AUSSM blocks. The UEA tasks feature much longer

Model	Mean Absolute Error ↓
Informer	0.731
LogTrans	0.773
LSTMa	1.109
LSTnet	0.757
S4	0.578
LinOSS	0.508 ³
Mamba	0.464 ²
AUSSM Hybrid	0.342¹

Table 3: **Hybrid AUSSM+Mamba achieves state-of-the-art performance on long time-series weather forecasting benchmark.** We evaluate AUSSM against 7 different models on the challenging weather forecasting benchmark, where climate variables are forecasted 720 timesteps into the future. AUSSM Hybrid achieves state-of-the-art performance on the task, improving on the base Mamba model and all the other models.

sequences than the algorithmic benchmark, with lengths ranging from 405 in the Heartbeat dataset to over 17,000 in the Worms dataset. For regression, we use the challenging Weather dataset where climate variables are forecasted 720 steps into the future given a window of 720 timesteps. These benchmarks present a more realistic and diverse set of challenges, which includes physiological signals, chemical concentrations, motion data, and climate, each requiring the model to capture both local and global temporal dependencies.

For the UEA benchmarks and the weather dataset, we used identical hyperparameter strategies to those used by the models we compare against. During testing, we found that previous works used five randomly chosen seeds to evaluate the test performance. This is not easily reproducible as the particular choice of the seeds influences the specific test datasets that are chosen for evaluation and may produce biased results. We instead use a statistically rigorous technique where the best hyperparameter model is chosen based on the validation set performance on five random seeds, and the test accuracy is evaluated on random train-test splits on the selected model with 20 different seeds to produce better test accuracy estimates. We scaled test accuracies with the baseline and report the results in Table 2. The hybrid AUSSM+Mamba model achieves substantial improvements over the partially adaptive Mamba SSM on average, even under the modified testing protocol. The results demonstrate that the improved expressivity of AUSSM carries over to real-world tasks when appropriately combined with the stability and inductive biases of partially adaptive models. Notably, the hybrid model achieves these results while maintaining high efficiency: all experiments except EigenWorms were run on a single NVIDIA 2080 Ti GPU with 11 GB of VRAM, in contrast to the large-scale hardware (e.g., 100 GB A100 GPUs) typically used for long-sequence modeling. The Eigenworms dataset was trained on an L4 GPU with 23 GB VRAM.

6 Discussion

This work addresses the tradeoff in state space modeling between expressivity and scalability. Existing SSMs like Mamba are scalable but limited in expressivity due to fixed or partially adaptive recurrence. We introduce the Adaptive Unitary State Space Model (AUSSM), which uses input-dependent skew-symmetric recurrence to achieve both unitary evolution and high expressivity. Theoretically, AUSSM can implement modulo counters and simulate a broad class of regular languages, maximizing expressivity among diagonal SSMs when combined with Mamba under the Krohn–Rhodes framework. To ensure scalability, we develop a separable convolution formulation and a custom CUDA kernel, enabling linear-time training despite full adaptivity. Empirically, AUSSM achieves strong performance on symbolic reasoning tasks and serves as an effective drop-in enhancement to Mamba for long-range sequence modeling. Together, these results suggest that adaptive unitary recurrence is a powerful inductive bias for both symbolic and continuous sequence tasks.

Limitations. Our approach relies on the assumption that recurrent matrices are simultaneously diagonalizable, limiting the ability to express languages beyond solvable regular languages. While the separable kernel improves scalability, the per-step cost remains higher than fully LTI models.

Hybrid AUSSM+Mamba models show promise, but the best strategy for combining blocks is not yet well understood. Finally, due to resource limitations, our evaluations are limited to modest-scale tasks; further validation on foundation-model-scale benchmarks is needed.

7 Acknowledgements

We thank Reda Boumasmoud for his input and suggestions on an earlier draft of this manuscript. T.A.K. acknowledges the Kempner Institute for the Study of Natural and Artificial Intelligence at Harvard University for funding during work on this article. T.J.S. acknowledges funding from ONR N00014-23-1-2069. A.K. and H.T.S. acknowledges NSF for EAGER: Neural Networks that Temporally Change (NOTCH).

References

- [1] Abhimanyu Dubey, Abhinav Jauhri ..., and Zhiwei Zhao. The llama 3 herd of models. *ArXiv*, abs/2407.21783, 2024.
- [2] Gemma Team Morgane Riviere, Shreya Pathak ..., and Alek Andreev. Gemma 2: Improving open language models at a practical size. *ArXiv*, abs/2408.00118, 2024.
- [3] OpenAI Josh Achiam, Steven Adler, Sandhini Agarwal ..., and Barret Zoph. Gpt-4 technical report. 2023.
- [4] Xihao Piao, Zheng Chen, Taichi Murayama, Yasuko Matsubara, and Yasushi Sakurai. Fredformer: Frequency debiased transformer for time series forecasting. *Proceedings of the 30th ACM SIGKDD Conference on Knowledge Discovery and Data Mining*, 2024.
- [5] Haoyi Zhou, Shanghang Zhang, Jieqi Peng, Shuai Zhang, Jianxin Li, Hui Xiong, and Wancai Zhang. Informer: Beyond efficient transformer for long sequence time-series forecasting. In *Proceedings of the AAAI conference on artificial intelligence*, volume 35, pages 11106–11115, 2021.
- [6] Noelia Ferruz, Steffen Schmidt, and Birte Höcker. ProtGPT2 is a deep unsupervised language model for protein design. *Nature Communications*, 13(1):4348, July 2022.
- [7] Feyza Duman Keles, Pruthvi Mahesakya Wijewardena, and Chinmay Hegde. On the computational complexity of self-attention. In *International conference on algorithmic learning theory*, pages 597–619. PMLR, 2023.
- [8] Albert Gu, Isys Johnson, Karan Goel, Khaled Saab, Tri Dao, Atri Rudra, and Christopher Ré. Combining recurrent, convolutional, and continuous-time models with linear state space layers. *Advances in neural information processing systems*, 34:572–585, 2021.
- [9] Albert Gu, Tri Dao Goel, Kevin Rusch, Sam Shleifer, Atri Ahmed, Kaushik Dubey, Hatem Awadalla, William Kuszmaul, and Ameen Mohamed. Efficiently modeling long sequences with structured state spaces. In *International Conference on Learning Representations (ICLR)*, 2022.
- [10] Albert Gu and Tri Dao. Mamba: Linear-time sequence modeling with selective state spaces. *ArXiv*, abs/2312.00752, 2023.
- [11] Yash Sarrof, Yana Veitsman, and Michael Hahn. The expressive capacity of state space models: A formal language perspective. In *The Thirty-eighth Annual Conference on Neural Information Processing Systems (NeurIPS 2024)*, June 2024.
- [12] Dianlin Zhang. *A Linear Time-varying Model for Nonlinear Systems*. PhD thesis, Rice University, 1969.
- [13] Sepp Hochreiter, Yoshua Bengio, Paolo Frasconi, Jürgen Schmidhuber, et al. Gradient flow in recurrent nets: the difficulty of learning long-term dependencies, 2001.

- [14] Zachary W Davis, Gabriel B Benigno, Charlee Fletterman, Theo Desbordes, Christopher Steward, Terrence J Sejnowski, John H. Reynolds, and Lyle Muller. Spontaneous traveling waves naturally emerge from horizontal fiber time delays and travel through locally asynchronous-irregular states. *Nature Communications*, 12(1):6057, 2021.
- [15] Arjun Karuvally, Terrence Sejnowski, and Hava T Siegelmann. Hidden traveling waves bind working memory variables in recurrent neural networks. In Ruslan Salakhutdinov, Zico Kolter, Katherine Heller, Adrian Weller, Nuria Oliver, Jonathan Scarlett, and Felix Berkenkamp, editors, *Proceedings of the 41st International Conference on Machine Learning*, volume 235 of *Proceedings of Machine Learning Research*, pages 23266–23290. PMLR, 21–27 Jul 2024.
- [16] Lyle Muller, Frederic Chavane, John Reynolds, and Terrence J Sejnowski. Cortical travelling waves: mechanisms and computational principles. *Nature Reviews Neuroscience*, 19(5):255–268, 2018.
- [17] Mark M. Churchland, John P Cunningham, Matthew T. Kaufman, Justin D. Foster, Paul Nuyujukian, Stephen I. Ryu, and Krishna V. Shenoy. Neural population dynamics during reaching. *Nature*, 487:51 – 56, 2012.
- [18] Antonio Orvieto, Samuel L Smith, Albert Gu, Anushan Fernando, Caglar Gulcehre, Razvan Pascanu, and Soham De. Resurrecting recurrent neural networks for long sequences. In *International Conference on Machine Learning*, pages 26670–26698. PMLR, 2023.
- [19] Antonio Orvieto, Soham De, Caglar Gulcehre, Razvan Pascanu, and Samuel L Smith. Universality of linear recurrences followed by non-linear projections: finite-width guarantees and benefits of complex eigenvalues. *arXiv preprint arXiv:2307.11888*, 2023.
- [20] T. Konstantin Rusch and Daniela Rus. Oscillatory state-space models. *ArXiv*, abs/2410.03943, 2024.
- [21] Heithem Boufrioua and Boubekour Boukhezzar. Gain scheduling: A short review. In *2022 2nd International Conference on Advanced Electrical Engineering (ICAEE)*, pages 1–6, 2022.
- [22] Luca Zancato, Arjun Seshadri, Yonatan Dukler, Aditya Sharad Golatkar, Yantao Shen, Benjamin Bowman, Matthew Trager, Alessandro Achille, and Stefano Soatto. B’mojo: Hybrid state space realizations of foundation models with eidetic and fading memory. *Advances in Neural Information Processing Systems*, 37:130433–130462, 2024.
- [23] Kenneth Krohn and John Rhodes. Algebraic theory of machines. i. prime decomposition theorem for finite semigroups and machines. *Transactions of the American Mathematical Society*, 116:450–464, 1965.
- [24] Bingbin Liu, Jordan T. Ash, Surbhi Goel, Akshay Krishnamurthy, and Cyril Zhang. Transformers learn shortcuts to automata. In *The Eleventh International Conference on Learning Representations*, 2023.
- [25] Riccardo Grazi, Julien Siems, Jörg K.H. Franke, Arber Zela, Frank Hutter, and Massimiliano Pontil. Unlocking state-tracking in linear RNNs through negative eigenvalues. In *The Thirteenth International Conference on Learning Representations*, 2025.
- [26] N. Chomsky and M.P. Schützenberger. The algebraic theory of context-free languages*. In P. Braffort and D. Hirschberg, editors, *Computer Programming and Formal Systems*, volume 35 of *Studies in Logic and the Foundations of Mathematics*, pages 118–161. Elsevier, 1963.
- [27] David S. Dummit and Richard M. Foote. *Abstract algebra*. Wiley, New York, 3rd ed edition, 2004.
- [28] William Merrill, Jackson Petty, and Ashish Sabharwal. The illusion of state in state-space models. In *Proceedings of the 41st International Conference on Machine Learning, ICML’24*. JMLR.org, 2024.
- [29] Tri Dao and Albert Gu. Transformers are ssms: Generalized models and efficient algorithms through structured state space duality. *arXiv preprint arXiv:2405.21060*, 2024.

- [30] Howard Anton and Chris Rorres. *Elementary linear algebra: applications version*. John Wiley & Sons, 2013.
- [31] Guy E. Blelloch. *Vector models for data-parallel computing*. 1990.
- [32] Maximilian Beck, Korbinian Poppel, Markus Spanring, Andreas Auer, Oleksandra Prudnikova, Michael K Kopp, Günter Klambauer, Johannes Brandstetter, and Sepp Hochreiter. *xlstm: Extended long short-term memory*. *ArXiv*, abs/2405.04517, 2024.
- [33] Benjamin Walker, Andrew D. McLeod, Tiexin Qin, Yichuan Cheng, Haoliang Li, and Terry Lyons. *Log neural controlled differential equations: The lie brackets make a difference*. *ArXiv*, abs/2402.18512, 2024.
- [34] Oded Maler. *On the krohn-rhodes cascaded decomposition theorem*. In *Time for Verification: Essays in Memory of Amir Pnueli*, pages 260–278. Springer, 2010.
- [35] István Babcsányi. *Automata with finite congruence lattices*. *Acta Cybernetica*, 18(1):155–165, 2007.
- [36] David B Salkoff, Edward Zagher, and David A McCormick. *Propagation of traveling waves in the visual cortex requires microcircuit coordination*. *Neuron*, 105(4):708–719.e5, 2020.
- [37] Richard Brent, Colin Percival, and Paul Zimmermann. *Error bounds on complex floating-point multiplication*. *Mathematics of Computation*, 76(259):1469–1481, 2007.
- [38] Karl-Heinz Zimmermann. *On krohn-rhodes theory for semiautomata*. *arXiv preprint arXiv:2010.16235*, 2020.
- [39] John Hewitt, Michael Hahn, Surya Ganguli, Percy Liang, and Christopher D. Manning. *RNNs can generate bounded hierarchical languages with optimal memory*. In Bonnie Webber, Trevor Cohn, Yulan He, and Yang Liu, editors, *Proceedings of the 2020 Conference on Empirical Methods in Natural Language Processing (EMNLP)*, pages 1978–2010, Online, November 2020. Association for Computational Linguistics.
- [40] Thomas H. Cormen, Charles E. Leiserson, Ronald L. Rivest, and Clifford Stein. *Introduction to Algorithms, Third Edition*. The MIT Press, 3rd edition, 2009.

A Limitations of Non-Adaptive/Partially Adaptive SSMs

The expressivity of different classes of SSMs is defined by the types of dynamical systems and formal languages they are able to simulate. Appendix D analyzes the formal language expressivity and limitations of different classes of SSMs. In this section, we analyze expressivity related to different kinds of dynamical systems. First, we show that in line with Figure 1, SSM expressivity can be arranged in the order $\text{LTI real spectra} \subset \text{LTI complex} \subset \text{LTV partial} \subset \text{LTV}$. The models that have higher expressivity can simulate the models lower in the expressivity scale. Since $\text{LTV w unitary spectra}$ cannot be arranged precisely in this scale, we show an example of a class of multiscale processes that a partial LTV model like Mamba cannot simulate in a fixed hidden state and layer limits.

Expressivity of Single Block SSMs The dynamical systems that can be simulated by single block SSMs without non-linearities can be arranged in the order $\text{LTI real spectra} \subset \text{LTI complex} \subset \text{LTV partial} \subset \text{LTV}$.

Proof: For the proof, we start with the most general LTV SSM and show that the next lower class SSM is a special case. We do the same for all the subsequent SSM classes in the expressivity chain.

The single block LTV SSM has the following discrete form:

$$\begin{cases} \frac{dx(t)}{dt} = \exp(\Delta_t A_t) x(t) + \Delta_t B_t u(t), \\ y(t) = C_t x(t). \end{cases}$$

The next lower class of ssm: LTV partial has the following form

$$\begin{cases} \frac{dx(t)}{dt} = \exp(\Delta_t A) x(t) + \Delta_t B_t u(t), \\ y(t) = C_t x(t). \end{cases}$$

Note here that the Δ_t is a scalar that varies with time, but A is a fixed matrix. This can be derived as an instance of the LTV with $A_t = \Delta_t A$ where the equivalence between the two holds only in the case where the dimensionality of the SSM is 1. Similarly, the next lower class LTI complex has the following form

$$\begin{cases} \frac{dx(t)}{dt} = \exp(\Delta A) x(t) + \Delta B u(t), \\ y(t) = C x(t). \end{cases}$$

This is an instance of the LTV partial with $\Delta_t = \Delta, B_t = B$ and $C_t = C$, which means all the matrices are time invariant. The final class LTI real spectra is an instance of LTI Complex where the eigenvalues are further restricted to have 0 angle in the imaginary plane.

LTV is the most general class, but it is computationally infeasible to simulate the most general case. The non-diagonalizability of general matrix classes requires performing a full $O(n^3)$ matrix computation at each time step. Hence $\text{LTV w unitary spectra}$ with simultaneously diagonalizable unitary matrices is chosen as a principled middle ground. It is, however, not instantly apparent how $\text{LTV w unitary spectra}$ compares against LTV partial . To illustrate the difference, we introduce an example of a multi-timescale process.

Multi-timescale features: A time-series $u(t) \in \mathbb{R}$ is said to have multi-timescale features if the hidden state can be factorized into the following form ³

$$x(t+1) = \begin{pmatrix} f(t) & 0 \\ 0 & g(t) \end{pmatrix} x(t).$$

Where $f(t) \in \mathbb{C}, g(t) \in \mathbb{C}$ are general complex valued time varying functions and $f(t) \neq cg(t)$ for some constant c . That is, the timeseries exhibits at least two *independent* features denoting two different timescales.

partial LTV SSMs in multi-timescale timeseries: partial LTV SSMs are not able to represent multi-timescale features in data.

³the results trivially extend to systems with more than 2 dimensions

Proof: The proof is by contradiction. If partial LTV SSMs are able to solve multi-timescale timeseries, the following $\begin{pmatrix} f(t) & 0 \\ 0 & g(t) \end{pmatrix} = \Delta_t A$ is true. Solving the system for A leads to a constraint on $f(t) = cg(t)$ where c is some constant. This is true only when one of the functions is a constant multiple of the other, that is *the two functions are dependent and have the same timescale (with a possible constant factor difference)*.

LTV w unitary spectra SSMs in multi-timescale timeseries: LTV w unitary spectra SSMs can represent multi-timescale features in data as long as the $f(t), g(t) \in \exp(i\theta)$ where $\theta \in [-\pi, \pi]$. $f(t), g(t)$ can be independent.

Proof: We first substitute $f(t) = \exp(i\theta^f(t))$ and $g(t) = \exp(i\theta^g(t))$. The resulting dynamical system has $f(t)$ and $g(t)$ as eigenvalues, which have unit magnitude themselves. This is the definition of LTV w unitary spectra.

To summarize, if f and g are independent (e.g., $f(t) = t^2, g(t) = t$), then the partial LTV system cannot represent the multi-timescale features in the hidden state. On the other hand, LTV w unitary spectra imposes a weaker constraint where the only requirement is that $f(t)$ and $g(t)$ are constrained to the unit circle in the imaginary plane; the timescales of the two variables can be independent.

B AUSSM Derivation

We derive the AUSSM from a controlled and adaptive version of the skew-symmetric ODE used in the jPCA procedure in computational neuroscience, given below. The skew-symmetric ODE is first discretized using the Zero Order Hold procedure and then parameterized in polar coordinates. The steps to obtain the final AUSSM formulation are provided below.

$$\begin{cases} \frac{dx(t)}{dt} = A_t x(t) + B u(t), \\ y(t) = C x(t). \end{cases} \quad (9)$$

The above ODE is discretized following the Zero Order Hold procedure with a step size of Δ_t (note that the step size is also time varying like the recurrent matrix)

$$\begin{cases} x(t) = \exp(\Delta_t A_t) x(t-1) + \Delta_t B u(t), \\ y(t) = C x(t). \end{cases} \quad (10)$$

The convolution form of the above system can be derived from this recurrence as shown below (assuming $x(0) = 0$)

$$y(1) = C \Delta_1 C B u(1) \quad (11)$$

$$y(2) = C \exp(\Delta_2 A_2) \Delta_1 B u(1) + \Delta_2 C B u(2) \quad (12)$$

$$\vdots \quad (13)$$

$$y(t) = C \sum_{k=1}^{t-1} \left(\prod_{l=k+1}^t \exp(\Delta_l A_l) \right) \Delta_k B u(k) + \Delta_t C B u(t) \quad (14)$$

Note that without additional assumptions on A , the matrix exponential and the repeated products cannot be simplified further which can result in computationally inefficient approaches to compute the output. We draw motivation from the use of structured matrices in efficient SSM implementations and propose that A_t belongs to a class of matrices that are simultaneously diagonalizable with the same basis. Let this diagonalizable basis be P .

$$y(t) = C \sum_{k=2}^{t-1} P \left(\prod_{l=k+1}^{t-1} \exp(\Delta_l \Lambda(A_l)) \right) P^{-1} \Delta_k B u(k) + \Delta_t C B u(t), \quad (15)$$

where $\Lambda(A_l)$ is the diagonal matrix with the eigenvalues of A_l on the diagonal. Now, the repeated matrix product has a simplified form as shown below.

$$y(t) = C P \sum_{k=2}^{t-1} \left(\exp \left(\sum_{l=k+1}^{t-1} \Delta_l \Lambda(A_l) \right) \right) P^{-1} \Delta_k B u(k) + \Delta_t C B u(t), \quad (16)$$

For a new set of B' and C' such that $C' = CP$ and $B' = P^{-1}B$, we get

$$y(t) = C' \sum_{k=2}^{t-1} \left(\exp \left(\sum_{l=k+1}^{t-1} \Delta_l \Lambda(A_l) \right) \right) \Delta_k B' u(k) + \Delta_t C' B' u(t), \quad (17)$$

The above equation undergoes one additional simplification, which reveals the unitarity of the discrete dynamical system. Since A_l is a skew-symmetric matrix, the eigenvalues $\Lambda(A_l)$ are purely imaginary, meaning the above equation simplifies further in the polar form of A_l .

$$y(t) = C' \sum_{k=2}^{t-1} \left(\exp \left(\mathbf{i} \sum_{l=k+1}^{t-1} \Delta_l \Im(\Lambda(A_l)) \right) \right) \Delta_k B' u(k) + \Delta_t C' B' u(t), \quad (18)$$

where $\mathbf{i}^2 = -1$ is the complex iota and $\Im(\cdot)$ is the function that obtains the imaginary component of a complex number. Since C' and B' are also complex due to the multiplication with P , we use polar forms for them too to finally obtain

$$y(t) = R_C \exp(\mathbf{i}\theta_C) \sum_{k=2}^{t-1} \left(\exp \left(\mathbf{i} \sum_{l=k+1}^{t-1} \Delta_l \Im(\Lambda(A_l)) \right) \right) \Delta_k R_B \exp(\mathbf{i}\theta_B) u(k) + \Delta_t R_C \exp(\mathbf{i}\theta_C) R_B \exp(\mathbf{i}\theta_B) u(t). \quad (19)$$

To handle a d -dimensional input, this formulation is replicated d times for each input dimension. For adaptivity, we use where $\Lambda(\Delta_l A_l)_j = \sum_r \chi_{jr} u_r(l) + \chi_j^{\text{bias}}$ and $\Delta_{lj} = \sum_r \chi_{jr}^\Delta u_r(l) + \chi_j^{\Delta \text{bias}}$. We use the above formulation in our experiments and parameterize the following for learning: $R_C, \theta_C, R_B, \theta_B, \chi_{jr}, \chi_j^{\text{bias}}, \chi_j^{\Delta \text{bias}}, \chi_{jr}^\Delta$.

C Eigenvalue Analysis

Lemma 3 (Exponential of a Skew-Symmetric Matrix is Orthogonal). *Let $A \in \mathbb{R}^{n \times n}$ be a real skew-symmetric matrix, i.e., $A^\top = -A$. Then the matrix exponential $\exp(\Delta A)$ is orthogonal for any $\Delta \in \mathbb{R}$, i.e.,*

$$\exp(\Delta A)^\top \exp(\Delta A) = I.$$

Proof. Let $U = \exp(\Delta A)$. Then,

$$U^\top = (\exp(\Delta A))^\top = \exp(\Delta A^\top) = \exp(-\Delta A),$$

since $A^\top = -A$. Therefore,

$$U^\top U = \exp(-\Delta A) \exp(\Delta A) = \exp(0) = I,$$

which shows that U is orthogonal. \square

Lemma 4 (Marginal Stability of Discrete-Time Dynamics). *Let $A \in \mathbb{R}^{n \times n}$ be a real skew-symmetric matrix and define $\Phi = \exp(\Delta A)$ for some $\Delta > 0$. Then all eigenvalues of Φ lie on the complex unit circle. In particular, the discrete-time linear system*

$$x(t) = \Phi x(t-1)$$

is marginally stable.

Proof. The eigenvalues of a real skew-symmetric matrix A are purely imaginary, i.e., $\lambda_j = i\omega_j \in i\mathbb{R}$. The eigenvalues of $\Phi = \exp(\Delta A)$ are then

$$\mu_j = \exp(\Delta \lambda_j) = \exp(i\Delta \omega_j),$$

which all lie on the complex unit circle since $|\exp(i\theta)| = 1$ for all $\theta \in \mathbb{R}$. Hence, the system exhibits marginal stability. \square

Lemma 5 (Norm Preservation under Skew-Symmetric Dynamics). *Let $A \in \mathbb{R}^{n \times n}$ be a real skew-symmetric matrix, and let $\Phi = \exp(\Delta A)$. Then for any $x \in \mathbb{R}^n$,*

$$\|\Phi x\|_2 = \|x\|_2.$$

Hence, the transformation does not amplify or diminish the norm of the state vector, preventing both gradient explosion and vanishing during backpropagation through time.

Proof. Since Φ is orthogonal by Lemma 1, we have:

$$\|\Phi x\|_2^2 = (\Phi x)^\top (\Phi x) = x^\top \Phi^\top \Phi x = x^\top x = \|x\|_2^2.$$

Taking the square root yields $\|\Phi x\|_2 = \|x\|_2$. \square

Lemma 6 (Input-Modulated Rotation Frequencies via Skew-Symmetric Generator). *Let $A : \mathbb{R} \rightarrow \mathbb{R}^{n \times n}$ be a smooth function such that $A(u)$ is skew-symmetric for all $u \in \mathbb{R}$. Then for each $u \in \mathbb{R}$, all eigenvalues of $A(u)$ lie on the imaginary axis, and the eigenvalues of the discrete-time transition matrix $\Phi(u) = \exp(\Delta A(u))$ lie on the complex unit circle.*

Furthermore, the eigenvalues of $A(u)$ depend continuously on u , and thus the angular frequency of state-space rotation is smoothly and directly modulated by the input.

Proof. Let $A(u) \in \mathbb{R}^{n \times n}$ be skew-symmetric for all $u \in \mathbb{R}$, i.e., $A(u)^\top = -A(u)$. It is a well-known result from linear algebra that real skew-symmetric matrices have purely imaginary eigenvalues or zero.

Let $\lambda_j(u) \in \mathbb{C}$ be an eigenvalue of $A(u)$. Since $A(u)$ is real and skew-symmetric, $\lambda_j(u) = i\omega_j(u)$ for some $\omega_j(u) \in \mathbb{R}$, and the eigenvalues come in complex-conjugate pairs if nonzero.

Now, consider the discrete-time transition matrix:

$$\Phi(u) := \exp(\Delta A(u)).$$

Because the exponential of a skew-symmetric matrix is orthogonal (by Lemma 1), $\Phi(u)$ is an orthogonal matrix. The eigenvalues of an orthogonal matrix with determinant 1 lie on the complex unit circle, i.e.,

$$|\mu_j(u)| = 1 \quad \text{for all eigenvalues } \mu_j(u) \text{ of } \Phi(u).$$

Furthermore, the eigenvalues of $\Phi(u)$ are given by

$$\mu_j(u) = \exp(\Delta \lambda_j(u)) = \exp(i\Delta \omega_j(u)),$$

so their arguments (i.e., angular velocities) are precisely modulated by the real-valued frequencies $\omega_j(u)$, which in turn depend on the input u .

To show that the rotational frequencies vary continuously with u , recall that the eigenvalues of a smooth matrix function $A(u)$ depend continuously on u , provided that $A(u)$ has distinct eigenvalues or that perturbations are small (which holds generically due to the structure of skew-symmetric matrices). Since $A(u)$ is assumed to be smooth, all $\omega_j(u)$ vary continuously with u , and therefore so do the corresponding angles $\Delta \omega_j(u)$ of the discrete-time rotation matrix. \square

D Formal Language Expressivity

Our formal expressivity analysis uses the setting and proofs of [11] as a starting point. That is, we abstract away architectural details without loss of generality, and directly work with the already discretized form of the SSM. We assume fixed-precision floating-point arithmetic. Here, we briefly reiterate a somewhat abstract definition of our SSM to simplify the expressivity proofs.

Definition 1 (SSM layer). *A single SSM layer is a sequence-to-sequence map $\mathbb{R}^d \rightarrow \mathbb{R}^d$, $(u_t) \mapsto (y_t)$ for $t \in [T]$ for sequence length T . It is defined recurrently by*

$$x_t = A_t \circ x_{t-1} + B_t \tag{20}$$

where \circ is elementwise multiplication, $x_0 \in \mathbb{C}^m$ with $m = n \cdot d$, and $A, B: \mathbb{R}^d \rightarrow \mathbb{C}^m$ are smooth, input-dependent maps with $A_t = A(u_t)$ and $B_t = B(u_t)$. Note that A already subsumes the

discretization variable Δ , which is itself a function of the input, as introduced in [9]. The output of the layer is computed as

$$y_t = \phi(x_t, u_t) \quad (21)$$

where

$$\phi: \mathbb{C}^m \times \mathbb{R}^d \rightarrow \mathbb{R}^d, \quad (x_t, u_t) \mapsto \text{Mix}_1(\Re(\text{Mix}_2(x_t, u_t)), u_t) \quad (22)$$

Mix_1 and Mix_2 contain linear maps and a non-linearity (either silu or softplus).⁴ Note that in our implementation, unlike [9], we do not apply normalization between the two Mix blocks but before the input enters the layer (see Def. 4). For ease of notation, we subsume C_t into Mix_2 without loss of generality. Mix_2 also usually contains a convolution of the input before the SSM recurrence, which we ignore in expressivity analyses following [11, Remark 18].

Definition 2 (Mamba layer). A Mamba layer is an SSM layer where A_t and B_t , are input-dependent and real-valued,⁵ and, additionally, $A_t \in \mathbb{R}^+$ is non-negative.

Definition 3 (AUSSM layer). An AUSSM layer is an SSM layer where B_t and C_t are fixed constant functions (not input dependent) and A_t is input dependent, complex valued, and each entry has unit magnitude, i.e.,

$$\forall j \in [d], \quad |A_{t,j}| = \sqrt{\Re(A_{t,j})^2 + \Im(A_{t,j})^2} = 1$$

Definition 4 (Full SSM). For a full SSM we usually stack multiple layers $(1, \dots, L)$ on top of each other, and indicate the layer we mean by a superscript, e.g., $x_t^{(\ell)}$ is the hidden state at time t in layer ℓ . The input to the first layer $u_t^{(1)}$ is some embedding of the input of the full SSM computed by some injective embedding function $e: \Sigma \rightarrow \mathbb{R}^d$, where Σ is the alphabet of possible input values at a single timestep, and the input to layer $\ell \in [L]$ for $\ell > 1$ is the normalized output of the previous layer $\ell - 1$:

$$u_t^{(\ell)} = \text{Norm}(y_t^{(\ell-1)}) \quad (23)$$

We use RMSNorm for the Norm , defined by

$$\text{RMSNorm}(x) = \frac{g \circ x}{\sqrt{\frac{1}{n} \sum_{i=1}^n x_i^2}} \quad (24)$$

where $x \in \mathbb{R}^n$ and $g \in \mathbb{R}^d$ is a learned gain parameter. Importantly, like [9], our implementation uses skip connections between consecutive layers, i.e., for

$$y^{(\ell)} = \phi(x_t, u_t) + y^{(\ell-1)} \quad (25)$$

The final layer applies another RMSNorm and then a final output function.

We now introduce some notions from automata theory that are necessary for our expressivity results.

Definition 5. A deterministic finite-state automaton (FSA) \mathcal{A} is a tuple (Σ, Q, δ) where Σ is an alphabet (finite, non-empty set), Q is a finite set of states and $\delta: Q \times \Sigma \rightarrow Q$ is a transition function. The transition function can be lifted from symbols to symbol sequences as

$$\delta: Q \times \Sigma^* \rightarrow Q, \quad \delta(q, \varepsilon) = q, \quad \delta(q, \sigma_{\leq t}) = (\delta(q, \sigma_{< t}), \sigma_t)$$

where ε is the empty string, Σ^* is the Kleene closure over Σ , and we use boldface to mark sequences of zero or more symbols from Σ^* .

The extended transition function δ forms a transformation monoid under composition, called the transition monoid of the FSA.

Definition 6. A set-reset automaton is an FSA whose transition function maps all states to a single state for each input symbol, that is, $\forall \sigma \in \Sigma, \exists p \in Q$ s.t.

$$\delta(q, \sigma) = p, \quad \forall q \in Q$$

Note that the transition monoid of a set-reset automaton is aperiodic [34].

⁴Here, $\text{silu}(x) = \frac{x}{1 + \exp(-x)}$ and $\text{softplus}(x) = x \log(1 + \exp(x))$

⁵Note that in Mamba, B_t is directly a function of the input while A_t is input dependent through Δ , which is itself a (non-linear) function of the input.

Definition 7. A cyclic permutation automaton is an automaton whose transitions are permutations over states, where every input symbol acts as some power of a fixed k -cycle with $k = |Q|$. That is, for every symbol $\sigma \in \Sigma$, the symbol-specific transition map $\delta_\sigma : Q \rightarrow Q$ is a bijection, and at least one of the symbols forms a cycle of order exactly k , i.e. for some $a \in \Sigma$, $\delta_a^k = \text{id}$ and $\delta_a^n \neq \text{id} \forall n \in [1, k-1]$. All other symbol-transition matrices are powers of the same k -cycle, i.e., $\forall b \in \Sigma, \delta_b = \delta_a^n$ for some $n \in [0, k-1]$, where $\delta_a^0 = \text{id}$.

The transition monoid of a k -cyclic permutation automaton is the cyclic group C_k [35].

We start by showing that our AUSSM architecture overcomes the limitation of most SSMs pointed out in [36] by showing that it can perform modulo counting, and therefore, can simulate cyclic permutation automata.

Lemma 1. For any $k \in \mathbb{Z}^+$, one can construct a single-layer AUSSM that counts modulo k , which means AUSSMs can simulate arbitrary cyclic permutation automata.

Proof. Let $\mathcal{A} = (\Sigma, Q, \delta)$ be a cyclic permutation automaton. Now we define the input alphabet of the AUSSM to be Σ and choose its hidden dimension to be $d = |\Sigma|$. Let $a \in \Sigma$ be the symbol whose transition function δ_a has order k . Then we set the parameters of the AUSSM as follows: Let $B(u) = 0 \forall u = e(\sigma), \sigma \in \Sigma$. Let $A(e(a)) = \exp(2\pi i/k)$. For each other symbol $b \in \Sigma$, we know there exists $m \in [0, k-1]$ such that $\delta_b = \delta_a^m$, so we can set $A(e(b)) = \exp(2\pi im/k)$. Now, there is a trivial isomorphism ψ between the values of x and the states of the FSA \mathcal{A} : Just define $\psi: \{\exp(2\pi in/k) \mid n \in [k]\} \rightarrow \mathbb{Z}/k\mathbb{Z}, \exp(2\pi in/k) \mapsto n$, which maps every hidden state to the corresponding state of the automaton (arranged in the order of cycle traversal by δ_a). Now there are n distinct possible hidden states which can be read out at finite precision. \square

A note on precision. In a realistic fixed-precision setting, floating-point operations introduce rounding errors when computing the exponential function and repeated products thereof. A single complex multiplication introduces an error of at most $\sqrt{5}\epsilon$ [37], where ϵ is the machine epsilon ($\epsilon = 2^{-53} \approx 10^{-16}$ in 64-bit double floating point precision). This means after N multiplications, the accumulated error is $\sqrt{5}\epsilon N$ in the worst case. Two adjacent k th roots of unity are separated by a $2\pi/k$ segment of the unit circle, so by the chord theorem, the distance between them is $\Delta = 2 \sin(\pi/k) \approx 2\pi/k$. Hence, approximations start overlapping if the accumulated error surpasses $\Delta/2$, which happens after

$$N \geq \frac{\Delta}{2\sqrt{5}\epsilon} \approx \frac{\pi}{\sqrt{5}\epsilon k} \approx \frac{1}{k} \cdot 10^{16}$$

for 64-bit double floating point precision. Even for modulo counters of up to a million, it would take 10 billion tokens for counts to be indistinguishable, which exceeds the sequence length of most datasets currently used in practice.⁶ If more precise counters are required, one could simply switch to 128-bit precision.

The second requirement for transcending the expressivity limits of common SSMs is the ability to implement cascade products of FSAs (see [23, 34, 38] for more details on cascade products):

Definition 8. Let $\mathcal{A}_1 = (\Sigma_1, Q_1, \delta_1), \mathcal{A}_2 = (\Sigma_2, Q_2, \delta_2)$ be FSAs such that $\Sigma_2 = Q_1 \times \Sigma_1$. Then the cascade product $\mathcal{A}_1 \circ \mathcal{A}_2$ is the FSA $\mathcal{C} = (\Sigma_1, Q_1 \times Q_2, \delta_c)$ with δ_c defined as

$$\delta_c((q_1, q_2), \sigma) = (\delta_2(q_1, (q_2, \sigma)), \delta_1(q_1, \sigma)) \quad (26)$$

Here, we use tuples of states taken from the state sets of the component FSAs to denote the state of the cascade. Intuitively, the state of the cascade at any given time is the combination of the states that the component FSAs are in at that point.

Note that for transitioning to the next state, \mathcal{A}_2 requires access to the state \mathcal{A}_1 was in before starting the current transition, meaning at time t , an FSA higher up in a cascade needs access to the state the lower-level FSAs were in at time $t-1$.

We will hence use the following crucial fact [11] used for constructing FSA cascade products in Mamba SSMs:

⁶For comparison, the human genome has around 3 billion base pairs.

Fact 2 (Sarrof et al. [11], Lemma 17). *For any alphabet Σ there exists a single-layer Mamba SSM such that the last-but-one input symbol can be read out from the hidden state at finite precision.*

We will also need the following fact about our hybrid architecture, allowing us to disregard the particular alternating ordering of layer types:

Note 1. *We can always add an idempotent Mamba or AUSSM layer in the cascade without changing the model's behavior. This can be done by setting the output projection of the SSM block in question to map everything to zero. Then the input to the next layer will just be the output of the last but one layer (via the skip connection). This means that for any Mamba or AUSSM with a specific behavior, there is a hybrid AUSSM+Mamba with the same behavior.*

Now we have the necessary building blocks to show that our construction fulfills the main requirement for increased expressivity, the ability to implement cascades of the two SSM layer types:

Lemma 2. *An SSM consisting of interleaved Mamba and AUSSM blocks (hybrid Mamba+AUSSM) can implement cascade products of automata simulated by Mamba SSMs and AUSSMs.*

Proof. We want to show that the hybrid Mamba+AUSSM architecture with alternating Mamba and AUSSM layers can implement cascade products of FSAs. In the following, we take a hybrid Mamba+AUSSM to mean a stack of alternating Mamba and AUSSM layers, ignoring the initial encoding and final normalization and output map. Without loss of generality, assume that the first layer is always an AUSSM layer, and the last layer is always a Mamba layer (we can achieve this by adding idempotent layers where necessary, see Note 1).

Also note that, by Note 1, any Mamba SSM and any AUSSM can be converted to an equivalent hybrid Mamba+AUSSM.

It remains to be shown that a hybrid Mamba+AUSSM can simulate the cascade of two FSAs simulated by hybrid Mamba+AUSSMs. This is simply an extension of [11, Lemma 19] to our hybrid Mamba+AUSSM architecture.

Let $\mathcal{A}_1 = (\Sigma_1, Q_1, \delta_1)$, $\mathcal{A}_2 = (\Sigma_2, Q_2, \delta_2)$ be FSAs such that $\Sigma_2 = Q_1 \times \Sigma_1$. Assume that there are hybrid Mamba+AUSSM models S_1, S_2 that map input sequences (x_1, x_2, \dots, x_T) to the sequences of states under A_1, A_2 , at finite precision.⁷

Let S_c be the hybrid Mamba+AUSSM we want to simulate the cascade $A_1 \circ A_2$. The lower layers of S_c are just the layers of S_1 . We add d dimensions that just copy the input via a skip connection. We then add a Mamba layer (preceded by an idempotent AUSSM layer) that reads out the second-to-last output of S_1 in new dimensions (by Fact 2), while again forwarding the input via the skip connection. Here, we also add a dummy dimension that is always 1, to avoid normalization making different inputs indistinguishable. Now we have the input and the second-to-last output of S_1 , corresponding to the last state of A_1 . Now the remaining layers of S_c are just those of S_2 , which take this input and compute the transition and state of A_2 , again adding dimensions such that the state of A_2 is separate from the state of A_1 and the input to the overall SSM. Now, S_c maps each w to the state sequence under $A_1 \circ A_2$, again at finite precision. This can be inductively extended to a cascade product of arbitrarily many FSAs. \square

Fact 3 (Consequence of Krohn-Rhodes Theorem [23] and the decomposition series of groups [27]). *Any solvable language is recognized by a cascade of set-reset and cyclic permutation automata.*

Corollary 1. *Hybrid Mamba+AUSSM can recognize any solvable language, that is, any regular language whose syntactic monoid does not contain non-solvable subgroups.*

Proof. By Lem. 1, an AUSSM can simulate cyclic permutation automata. By [11, Lem. 19], a Mamba SSM can simulate set-reset automata. By Lem. 2, hybrid AUSSM+Mamba can simulate a cascade of automata simulated by Mamba and AUSSM SSMs. Together with Fact 3, this means that hybrid AUSSM+Mamba can recognize any solvable language. \square

⁷Note here we implicitly assume a bijection exists between intervals on \mathbb{R}^d (the input at time t , x_t) and the alphabet symbols of the relevant FSA.

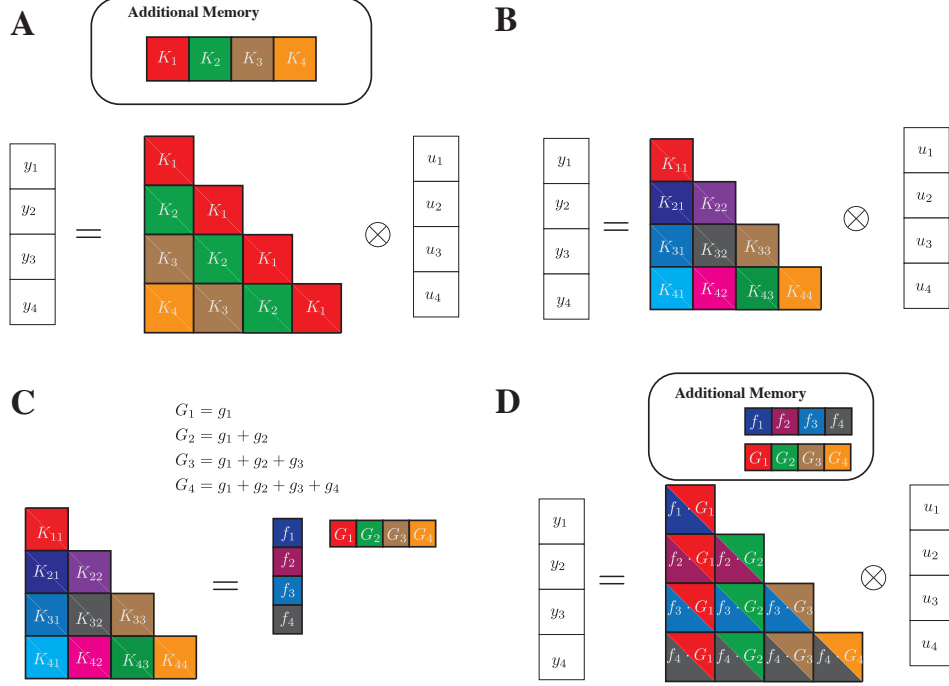


Figure 3: Space Complexity of SSM formulations: The figure illustrates an example convolution kernel for an SSM provided with four inputs at different timesteps (u_t). The convolution is visualized as a matrix multiplication operation over the input sequence. **A.** In LTI SSMs, the convolution kernel (K_1, K_2, K_3, K_4) is precomputed and applied to the input at different timesteps to obtain the output. **B.** In general LTV SSMs with time varying recurrence, the convolution kernel has $O(L^2)$ elements each unique to the input and output being considered at each timestep. The use of convolution in this scenario leads to quadratic complexity in space (akin to the transformers). **C.** In the separable convolution case, the quadratic matrix of the general SSM can actually be obtained by the outer product between f_t for each timestep and the cumulative sums of a function g_k independent of t . **D.** Computing the convolution kernel can be achieved in just an additional $O(2L)$ space.

The importance of counting for other tasks. Note that the ability to count modulo k does not just allow SSMs to model regular languages but also to approximate languages higher up on the Chomsky hierarchy. For example, it allows the recognition or generation of bounded Dyck languages, i.e., the correct parenthesization up to a certain depth (see [39] in the case of RNNs). Even context-sensitive language tasks can benefit from counting: For instance, sorting a sequence (the bucket sort task in §5) can be done by maintaining counters for all alphabet symbols and then outputting the symbols in order, according to their count (see counting sort and direct-address tables [40, Chapters 8 and 11]). Note that this works as long as the number of occurrences of any given symbol is smaller than the highest count expressible by the SSM, e.g., k when using modulo k counting.

E Complexity Analysis

SSMs leverage logarithmic complexity algorithms like FFT and parallel prefix sum to compute the convolution. Prior to this, the convolution kernel needs to be pre-computed and stored, which is the main bottleneck in computing the convolution. We will show below the space complexities for computing and storing the convolutions. Further, we show how the quadratic space complexity blowup of pure LTV systems can be managed using the separable convolution framework.

E.1 SSM Convolution

The convolution operation of a general SSM is given by the following

$$y(t) = \sum_{k \leq t} C_t (A_{t-1} \dots A_{k+2} A_{k+1}) B_k u(k) \quad (27)$$

There are two cases for the above convolution we consider:

Linear Time Invariant (LTI) : In the LTI case, the matrices in the SSM are constant over time and the following holds

$$y(t) = \sum_{k \leq t} C A^{t-1-k} B u(k) \quad (28)$$

Now, the convolution kernel $K(t, k) = C A^{t-1-k} B$ can be precomputed and since A^{t-k-1} is common for many settings of t and k for which their difference is constant, the weights can be shared. In fact, there are only $O(L)$ unique entries in the convolution kernel (see Figure 3 A). The other entries are duplicates of these entries. Once the convolution kernel is obtained, efficient algorithms like FFT or Parallel Scan can be used to compute the convolution in $O(\log L)$ time for each dimension, for a total of $O(L \log(L))$ time complexity. Therefore, the total time complexity for computing the kernel is $O(L \log L)$ with a space complexity of $O(L)$.

Linear Time Varying (LTV) : In the LTV case, the matrices in the SSM can vary over time. This introduces additional complexity in representing the convolution kernel in $O(L^2)$ space, matching the quadratic complexity of computing self-attention in transformers. The reason for the quadratic complexity is that the entries in the convolution kernel $K(t, k)$ are unique for each setting of t, k . In the case of separable convolution kernels (e.g. the case of simultaneously diagonalizable matrices), the resulting $K(t, k)$ matrix has a further rank-1 factorization (this is discussed in detail in the main text). This factorization enables the convolution kernel to be represented with only an additional $O(2L)$ memory, where the 2 factor comes from each vector element in the outer product.

E.2 Parallel Scan

The reason for precomputing the convolution kernel is that we can apply one of the fast convolution algorithms - FFT or parallel scan. In our case, we perform the parallel prefix sums for computing cumulative sums. Here, we analyze the time and space complexity of the parallel prefix sum (scan) algorithm, where the goal is to compute the prefix sums of an array $A = [a_0, a_1, \dots, a_{L-1}]$ such that the output array S satisfies

$$S_i = \sum_{j=0}^i a_j \quad \text{for } 0 \leq i, j < L. \quad (29)$$

We assume a parallel computation model such as the PRAM (Parallel Random Access Machine) or a shared-memory model, and we are given P processors.

The parallel prefix sum algorithm typically consists of two main phases:

1. **Upsweep phase (Reduction):** Build a binary tree over the array and compute partial sums from leaves to the root.
2. **Downsweep phase:** Propagate prefix sums from the root back down the tree to compute the final result.

Both phases traverse a binary tree structure of height $\log_2 L$, assuming for simplicity that L is a power of two. Each level of the tree can be processed in parallel.

Work. The total number of operations (work) in both phases is:

$$W(L) = \underbrace{(L-1)}_{\text{upsweep}} + \underbrace{(L-1)}_{\text{downsweep}} = 2L - 2 = \mathcal{O}(L). \quad (30)$$

This is the same amount of work as the sequential prefix sum algorithm, which confirms that the parallel algorithm is work-efficient.

Time Complexity with P Processors. Using Brent’s Theorem (work-span model), the parallel time T_P on P processors is bounded by:

$$T_P \leq \frac{W(L)}{P} + S(L) = \mathcal{O}\left(\frac{L}{P} + \log L\right). \quad (31)$$

This means that when the number of parallel processors grow in the sequence length according to $P = \Theta(L/\log L)$, the parallel prefix sum runs in optimal time $\mathcal{O}(\log L)$.

Space Complexity The space used by the algorithm includes:

- The original input array A , of size L .
- An auxiliary array to store intermediate results, typically of size L .
- Additional temporary variables per processor (constant per processor).

Hence, the total space complexity is:

$$\mathcal{O}(L + P) = \mathcal{O}(L) \quad (\text{since typically } P \leq L). \quad (32)$$

It is important to note that although the algorithm requires additional $\mathcal{O}(L)$ space for the auxiliary variables, the CUDA kernel implementation hides these variables within the multiprocessor registers and shared memory. As a result, this complexity does not show up in the plots of either Mamba or auSSM. Existing GPU hardware for the 2080ti enables parallel processing of sequences up to $L = 2048$. For longer sequences, the input is chunked into batches of $L = 2048$.

F Implementation

The theoretical analysis of the separable kernel formulation shows that the adaptive kernel can be implemented in only an additional linear space. However, the factor associated with the linear space is bdn where b is the batch size, d is the input dimension, and n is the hidden state dimension. In this section, we first show a Pytorch implementation of the AUSSM kernel and Mamba kernel that can be easily coded, with the higher cost of the constant factors. Next, we show how we implement the AUSSM kernel in practice so that the additional complexity is hidden within the computations of a CUDA kernel.

F.1 Pytorch

One of the most useful aspects of the theory of separable convolutions is that there is a relatively efficient Pytorch formulation for computing SSM kernels, even when the SSM is partially/fully time varying. However, the additional constant time penalty will be incurred. Nevertheless, the existence of such an implementation will still be interesting as it can enable fast prototyping of LTV SSMs, without dealing with the complexity of building a CUDA kernel. Here, we show two Pytorch implementations of the partial LTV Mamba kernel and the separable AUSSM kernel.

```

1 def mamba_ssm(u, dt, A, B, C, D, z):
2     """
3     params:
4         u: input Tensor (b,d,1)
5         dt: Delta Tensor (b,d,1)
6         A: Tensor (n)
7         B: Tensor (b,n,1)
8         C: Tensor (b,n,1)
9         D: Tensor (d)
10        z: Tensor (b,d,1)
11    Returns:
12        y: (b, d, 1)
13    """
14    A = einsum(A, dt, "n,bd1->bdn1")
15    G = torch.cumsum(axis=1)
16

```

```

17 g = einsum(exp(-G), dt, B, u, "bdnl,bdl,bnl,bdl->bdnl")
18 g = torch.cumsum(g, axis=-1)
19 f = einsum(C, exp(G), "bnl,bdnl->bdnl")
20
21 y = einsum(f, g, "bdnl,bdnl->bdl") + D * u
22 y = y * F.silu(z)
23
24 return y

```

The implementation of Mamba using the separable kernel formulation has less than 10 lines of Pytorch code. The Pytorch implementation of AUSSM is similar, except now we have to account for the time varying A matrix and B and C are relaxed.

```

1 def aussm(u, dt, chi, B, C, D, z):
2     """
3     params:
4         u: input Tensor (b,d,l)
5         dt: Delta Tensor (b,d,l)
6         chi: adaptivity matrix (d,n,d)
7         B: Tensor (n)
8         C: Tensor (n)
9         D: Tensor (d)
10        z: Tensor (b,d,l)
11    Returns:
12        y: (b,d,l)
13    """
14    A = einsum(chi, u, "dnr,blr->bldn")
15    A = einsum(dt, A, "bdl,bldn-bldn")
16    G = torch.cumsum(axis=1)
17
18    g = einsum(exp(-G), dt, B, u, "bdnl,bdl,n,bdl->bdnl")
19    g = torch.cumsum(g, axis=-1)
20    f = einsum(C, exp(G), "n,bdnl->bdnl")
21
22    y = einsum(f, g, "bdnl,bdnl->bdl") + D * u
23    y = y * F.silu(z)
24
25    return y

```

In this implementation, Mamba and Pytorch have the identical memory and time complexity as the hidden state is realized for both, albeit at only a fraction of the cost.

F.2 CUDA Kernel

In pure Pytorch, the additional complexity of realizing the hidden state is unavoidable, even though the computation does not have quadratic memory costs. The additional complexity of realizing the hidden state can be avoided by creating a CUDA kernel for the AUSSM equation. We use the following equation for the AUSSM, which we introduced in the main text:

$$y_{ti} = \Re \left[\sum_{k \leq t} \sum_j C_j \exp \left(\mathbf{i} \sum_{l \leq t} \theta_{A_{lij}} \right) \frac{\Delta_{ki} B_j}{\exp \left(\mathbf{i} \sum_{l \leq k} \theta_{A_{lij}} \right)} u_i(k) \right]. \quad (33)$$

Each thread of the CUDA implementation computes the array inside the nested summation, which results in $O(L)$ memory requirement for storing each of the variables (A, f, g) for the forward pass. These variables are not realized at the same time in the GPU memory, but in registers within the streaming multiprocessors (SM), each processor holding 4 to 16 items of each array. For the 2080Ti GPU we ran the CUDA kernel on, the allowable maximum sequence length that can be processed by the kernel was 2048 after which the register and shared memory costs start to show up. We found that this sequence length is ideal for the hardware and tasks we tested on. The separable convolution trick is not restricted by the hardware, and can scale well for GPUs that can be released in the future with larger registers and shared memory resources.

Table 4: Best Hyperparameters.

Task Group	Task	Layers	d	n	weight decay	learning rate
Algorithmic	repetition	ma	64	32	0.0	0.01
	bucket sort	am	64	32	0.0	0.01
	majority count	ma	64	32	0.1	0.01
	majority	ma	64	32	0.1	0.01
	solve equation	ma	64	32	0.0	0.01
	mod arith	am	16	8	0.0	0.01
	mod arith wo bra	ma	8	16	0.0	0.01
	cycle nav	ma	16	8	0.0	0.01
parity	ma	16	8	0.0	0.01	
Timeseries Classification	Heartbeat	ma	64	64	0.0	0.0001
	SCP1	amma	16	128	0.0	0.001
	SCP2	ma	16	128	0.0	0.0001
	Ethanol	ammama	16	64	0.001	0.00001
	Motor	ma	16	128	0.0	0.0001
Worms	amma	16	16	0.0	0.001	
Timeseries Regression	weather	ma	16	128	0.0	0.001

Backpropagation: For the CUDA kernel, we implemented a custom backpropagation operation. Implementing backpropagation requires the variables computed during the storage to be stored, which creates issues because the reason we are writing the CUDA kernel is so that we do not have to realize the memory-intensive hidden state. We therefore recompute the forward pass during backpropagation. The low complexity of implementing the AUSSM in CUDA means the recomputation does not incur a heavy penalty.

G Experiments

We conduct three sets of experiments - (1) to evaluate the time/memory complexities of the different AUSSM implementations, (2) to evaluate the performance of AUSSM in algorithmic tasks enabling insights into the expressive power, and (3) to evaluate real-world performance implications in a range of long time series benchmarks. For each of the tasks involving training models (2 and 3), we perform two pipeline processes to obtain the final test accuracies. The first pipeline is the training and model selection pipeline with only the training and validation sets that are preselected based on the same criteria prior literature used. The second pipeline is the test pipeline and is entirely separate and performed starting 10 days prior to paper submission to avoid model selection based on the test results. The classification tasks are evaluated using the scaled test accuracy metric, where the obtained accuracy values are scaled with respect to baseline performance of a uniform random distribution as shown below.

$$\text{scaled accuracy score} = \frac{\text{test accuracy score} - \text{baseline accuracy score}}{1 - \text{baseline accuracy score}}$$

All the models were run in a supercomputing cluster, where we used 40 2080Ti GPUs for all except the dataset Eigenworms dataset that required higher memory. This is the lowest GPU available in the cluster with at least a CUDA compute of 7.5 required to run the mamba and AUSSM CUDA kernels. For larger memory Eigenworms workload, we used the L4 GPU which has a VRAM of 23GB. Higher VRAM GPUs were available in the cluster, but they were in high demand and unnecessary as our optimized CUDA kernel was able to handle even the large scale tasks in modest hardware.

G.1 Scalability Evaluation

To evaluate scalability in a fair manner, we report only the time spent in computations, ignoring the latencies associated with moving variables between GPU and CPU. This provides a fair evaluation of the algorithmic performance. 5 runs are used to warm up the GPU before starting the evaluation

to remove transient start-up effects. The run-time values are averaged over 50 runs, where each run computes a forward and backward pass for each of the implementations. The peak memory used during each run is also similarly recorded and averaged for each of the 50 runs.

G.2 Algorithmic Tasks

For algorithmic tasks, we used the results from [32] for comparing against baseline models. We used a grid search for hyperparameter tuning with a grid search over $d \in \{8, 16, 32, 64\}$, $n \in \{8, 16, 32\}$, weight decay $\in \{0.0, 0.001, 0.01\}$, learning rate in $\{0.0001, 0.001, 0.01\}$ and 5 seeds. The batch size was fixed at 256. For pure AUSSM blocks, we tested networks with a depth of 2, 4, and 6. For hybrid AUSSM blocks, we tested all possible 2 block configurations of Mamba (represented as m) and AUSSM blocks (represented as a) - $\{ma, am, mm, aa\}$. For each of the evaluated algorithmic tasks, we randomly sampled 10000 samples from a train set up to 40 length sequences. The validation set is sampled independently from 40-256 sequence lengths and had 1,000 samples. The test set had 10,000 samples from sequences of up to 256 sequence lengths.

The tasks use the same vocabulary size and configuration used in [32]. Some samples from the tasks are shown below as a timeline. Here, the mask is applied on the output to determine the output of interest for computing the loss and output.

Task: repetition												
time	0	1	2	3	4	5	6	7	8	9	10	
input	3	5	0	7	3	ACT	3	5	0	7	3	
output	5	0	7	3	ACT	3	5	0	7	3	PAD	
mask	0	0	0	0	0	1	1	1	1	1	0	
Task: bucketsort												
time	0	1	2	3	4	5	6	7	8	9	10	
input	3	5	0	7	3	ACT	0	3	3	5	7	
output	5	0	7	3	ACT	0	3	3	5	7	PAD	
mask	0	0	0	0	0	1	1	1	1	1	0	
Task: modarithmicwobrases												
time	0	1	2	3	4	5	6	7	8	9	10	
input	0	*	2	-	6	-	7	-	0	=	5	
output	*	2	-	6	-	7	-	0	=	5	PAD	
mask	0	0	0	0	0	0	0	0	0	1	0	
Task: cyclenav												
time	0	1	2	3	4	5	6	7	8	9	10	
input	+1	STAY	+1	-1	+1	-1	-1	-1	+1	0	PAD	
output	STAY	+1	-1	+1	-1	-1	-1	+1	0	PAD	PAD	
mask	0	0	0	0	0	0	0	0	1	0	0	
Task: modarithmic												
time	0	1	2	3	4	5	6	7	8	9	10	
input	((3	-	3)	-	4)	=	3	
output	(3	-	3)	-	4)	=	3	PAD	
mask	0	0	0	0	0	0	0	0	0	1	0	
Task: solveequation												
time	0	1	2	3	4	5	6	7	8	9	10	
input	x	=	(2	+	1)	ACT	3	PAD	PAD	
output	=	(2	+	1)	ACT	3	PAD	PAD	PAD	
mask	0	0	0	0	0	0	0	1	0	0	0	
Task: parity												
time	0	1	2	3	4	5	6	7	8	9	10	
input	1	1	0	1	1	1	1	1	1	1	0	
output	1	0	1	1	1	1	1	1	1	0	0	
mask	0	0	0	0	0	0	0	0	0	0	1	
Task: majoritycount												
time	0	1	2	3	4	5	6	7	8	9	10	
input	45	56	51	43	51	34	10	46	54	44	56	
output	56	51	43	51	34	10	46	54	44	56	2	
mask	0	0	0	0	0	0	0	0	0	0	1	
Task: majority												
time	0	1	2	3	4	5	6	7	8	9	10	
input	45	56	51	43	51	34	10	46	54	44	56	
output	56	51	43	51	34	10	46	54	44	56	51	
mask	0	0	0	0	0	0	0	0	0	0	1	
Task: set												
time	0	1	2	3	4	5	6	7	8	9	10	
input	3	5	0	7	3	ACT	0	3	5	7	PAD	
output	5	0	7	3	ACT	0	3	5	7	PAD	PAD	
mask	0	0	0	0	0	1	1	1	1	0	0	

G.3 Time Series benchmark

For time series classification and regression benchmarks, we follow the train-validation protocol for model selection following prior works on the benchmark. For testing, we modified the procedure as the 5 arbitrary random seeds used to evaluate test performance in prior works may introduce unwanted biases due to the low number of random samples. Also, prior works used jax for implementations while we used Pytorch and the random seed does not create the same train-validation-test sets due to differences in the Pseudorandom number generators. We thus decided to evaluate on train-validation-test splits created with 20 different seeds. We anticipated that the higher samples help in providing a better estimation of the test accuracy than what the 5 arbitrary seeds provide. For each task, we performed a hyperparameter search over the following grid: $d \in \{16, 64, 128\}$, $n \in \{16, 64, 128\}$, learning rate $\in \{0.00001, 0.0001, 0.001\}$ and 5 different seeds for model selection. The model hyperparameters with the highest mean validation accuracy is chosen for evaluation in the test set.